NREL
NATIONAL RENEWABLE ENERGY LABORATORY

Investigation of Some Transparent Metal Oxides as Damp Heat Protective Coating for CIGS Solar Cells

Preprint

F.J. Pern, F. Yan, K. Zaunbrecher, B. To, J. Perkins, and R. Noufi

Presented at SPIE Optics + Photonics
San Diego, California
August 12–16, 2012

Conference Paper
NREL/CP-5200-54188
October 2012

Contract No. DE-AC36-08GO28308

Available electronically at http://www.osti.gov/bridge

Available for a processing fee to U.S. Department of Energy
and its contractors, in paper, from:

U.S. Department of Energy
Office of Scientific and Technical Information
P.O. Box 62
Oak Ridge, TN 37831-0062
phone: 865.576.8401
fax: 865.576.5728
email: mailto:reports@adonis.osti.gov

Available for sale to the public, in paper, from:

U.S. Department of Commerce
National Technical Information Service
5285 Port Royal Road
Springfield, VA 22161
phone: 800.553.6847
fax: 703.605.6900
email: orders@ntis.fedworld.gov
online ordering: http://www.ntis.gov/help/ordermethods.aspx

Cover Photos: (left to right) PIX 16416, PIX 17423, PIX 16560, PIX 17613, PIX 17436, PIX 17721

Printed on paper containing at least 50% wastepaper, including 10% post consumer waste.

INVESTIGATION of some transparent metal oxides as damp heat protective coating for CIGS solar cells

F.J. Pern*, F. Yan, K. Zaunbrecher, B. To, J. Perkins, and R. Noufi
National Center for Photovoltaics, National Renewable Energy Laboratory
1617 Cole Blvd., Golden, CO 80401, USA.

ABSTRACT

We investigated the protective effectiveness of some transparent metal oxides (TMO) on CIGS solar cell coupons against damp heat (DH) exposure at 85°C and 85% relative humidity (RH). Sputter-deposited bilayer ZnO (BZO) with up to 0.5-μm Al-doped ZnO (AZO) layer and 0.2-μm bilayer InZnO were used as "inherent" part of device structure on CdS/CIGS/Mo/SLG. Sputter-deposited 0.2-μm ZnSnO and atomic layer deposited (ALD) 0.1-μm Al_2O_3 were used as overcoat on typical BZO/CdS/CIGS/Mo/SLG solar cells. The results were all negative — all TMO-coated CIGS cells exhibited substantial degradation in DH. Combining the optical photographs, PL and EL imaging, SEM surface micro-morphology, coupled with XRD, I-V and QE measurements, the causes of the device degradations are attributed to hydrolytic corrosion, flaking, micro-cracking, and delamination induced by the DH moisture. Mechanical stress and decrease in crystallinity (grain size effect) could be additional degrading factors for thicker AZO grown on CdS/CIGS.

Key Words: Transparent metal oxide, Al-doped ZnO, amorphous InZnO, ZnSnO, ALD Al_2O_3, CIGS solar cell, damp heat stability

1. INTRODUCTION

Long-term performance reliability is critical for all kinds of photovoltaic (PV) modules, including thin-film CIGS. For terrestrial thin-film modules, the IEC 61646 qualification standard requires a stringent DH test at 85°C and 85% RH for 1000 h. A fairly high percentage of thin-film modules reportedly failed in this test [1], and Preiss et al. reported a 15% DH-test failure rate during certification process [2]. The CIGS cell component materials, including Mo, CIGS, and ZnO, have been shown to be DH-sensitive or unstable [3–7]. The CIGS solar cells and modules have also been shown to degrade in DH exposure [8-13]. Two main approaches can be employed to enhance DH resistance of CIGS solar cells and modules: (1) using a high-performance moisture barrier cover film [14-17] for flexible packaging and/or a moisture-blocking desiccant-type edge sealant tape for glass-glass laminates, and (2) a DH-resistant transparent metal oxide (TMO) coating, as previously discussed [18], directly on the CIGS either as a protective layer or as the conductive window layer being a part of the device structure. In the first approach, the moisture barrier films are already available commercially such as Vitex Systems' Barix films [19], along with two newer products: 3M's Ultra Barrier Solar Film [20] and DuPont's Ultrabarrier [21]. Commercial products of edge sealant tapes from, e.g., ADCO and TruSeal, have been used on both CIGS and CdTe thin-film modules. The DH-resistance property of edge sealant was recently reported by Kempe [22]. Coyle and coworkers studied the degradation kinetics and packaging requirements for flexible CIGS solar cells and modules and reported their findings on service life prediction [23-26]. Simulation has led to a popular view that the moisture-blocking property for the barrier films are required to provide a water vapor transmission rate (WVTR) as low as of 10^{-4} g/m^2-day or better to assure a >20-year service life [23-25].

While having a very low WVTR is highly desirable, however it may incite a small increase in module cost to incorporate such high-performance ― and potentially expensive ― barrier films. The WVTR requirement can likely be much relaxed, and so the module cost, for flexible package, if the CIGS solar cells can be "hardened" by using a moisture-blocking TMO coating on top of the cell structure (i.e., an "overcoat" method) or having an inherent DH-stable TMO as the window layer of the device structure (i.e., an "inherent" method). The "overcoat" approach is generally studied for CIGS with bi-layer ZnO window layer (i.e., BZO/CIGS), because the Al-doped ZnO (AZO) is highly prone to hydrolytic degradation upon DH exposure [4-7], which is attributed to be the lifetime-limiting factor for CIGSS mini-modules as reported by Feist et al. [12,13]. For example, we investigated overcoating NREL's "Mo/CIGS/CdS/i-Zno/AZO/AlNi

* john.pern@nrel.gov; phone 1 303 384-6615; fax 1 303 384-6490; www.nrel.gov/pv

grid" solar cells with SiO_xN_y deposited by PECVD [27,28] or with undoped SnO_2 by sputtering (NREL ROI #09-70) [7,29] with encouraging results. DeGroot and coworkers demonstrated good protective results when Si_3N_4/SiO_xN_y was applied with an ultrathin TaN layer to improve the adhesion [30]. Similar to our earlier work with sputtered SnO_2, Tosun et al. also showed recently that a semicrystalline SnO_2 overlayer, located either on top of the ZnO/ITO/AlNi grid or between ZnO/ITO and AlNi grids, can enhance the CIGS solar cell's DH endurance [31]. In the "inherent" approach, CIGS modules with an ITO window layer are a common choice; the ITO has been shown to be more DH-robust than ZnO [4,24]. Recently, Thompson et al. demonstrated that a CIGS device test structure with a 50-nm intrinsic ZnO (i-ZnO) and a 150-nm ITO window (WVTR ~2 x 10^{-3} g/m^2-day for the i-ZnO/ITO) *without* scribe lines, which was encapsulated with a 5-mil PET film (WVTR ~10 g/m^2-day), endured 2000 h DH exposure and retained 92% of initial device efficiency [32]. *With* scribe lines, greater efficiency loss was observed likely due to "edge" effect. These results clearly support the reasoning of having a "hardened" CIGS device structure to greatly enhance its DH resistance while reducing the WVTR requirement.

This work was a continuation of previous studies that aimed to identifying the means to largely improve the long-term performance reliability of CIGS solar cells by "hardening" the devices with either "inherent" or "overcoat" approach, or both in combination. For the "inherent" approach, we tested thicker AZO films (up to 0.5 μm) and amorphous bi-layer InZnO (~0.2 μm, a resistive plus a conductive layer) to replace the bilayer ZnO (BZO, an intrinsic ZnO and an AZO layer) as the window layer deposited as the protective transparent metal oxide (PTMO) on typical SLG/Mo/CIGS/CdS/BZO solar cells. Both were shown to be DH stable when deposited on glass substrates [6,7]. Partial results of the DH stability of CIGS solar cells made with thicker AZO layer were reported previously [33,34], and more details are summarized below and for comparison. For the "overcoat" approach, following a previous study using 0.1-μm SnO_2 as the PTMO [7,29], more work was performed with SnO_2 and an alloy of it co-sputtered on glass substrates under various deposition conditions; however, no overcoat of either oxide on CIGS cell coupons could be done due to prolonged system breakdown later. Two highly resistive oxides, amorphous ZnSnO (ZSO) by sputtering and Al_2O_3 (ALO) by atomic layer deposition (ALD), were investigated as overcoats.

2. EXPERIMENTAL

Sample preparations. The CIGS thin films were prepared by NREL's three-stage thermal coevaporation process on Mo-coated soda lime glass (SLG), followed by CBD CdS (~70 nm) and bilayer ZnO (BZO, i.e., AZO on 0.1-μm intrinsic ZnO layer) using the "standard" conditions. The thickness of the AZO layer was increased from the typical 0.12 μm to 0.24, 0.36, and ~0.50 μm, which would increase the ambient temperature over the substrates due to increased deposition time [33]. For making the solar cells with a-InZnO, a 3" x 3" piece of the CIGS film was first coated with CBD CdS before cutting into six 1" x 1.5" pieces. Four of the CIGS/CdS piece were coated with bi-layer a-InZnO (IZO), a high-resistance layer (≤ 0.1 μm) and a high-conductance layer (≤ 0.1 μm), at different sputtering conditions. One piece was coated with 0.22 μm BZO (i.e., the "standard" CIGS solar cells) and was used as control. After AlNi (3 μm/0.05 μm) contact grids were deposited by e-beam evaporation, photolithography was employed to define and isolate the devices with a cell area of 0.42 cm^2. For the "overcoat" samples, the "standard" CIGS cell coupons with BZO and AlNi grid, completed with isolated devices and external electrical connections soldered with thin Au wires [33,34], were coated over the entire surfaces with ~0.2 μm high-resistance a-ZSO at ambient temperature, or with ~0.1 μm ALO at 100°C in a customer-built ALD system. The BZO, IZO, ZSO, and ALD ALO thin films, termed as transparent metal oxide (TMO) herein, were also deposited on witness glass substrates for optical and other measurements. A set of the CIGS cell coupons with BZO of different AZO thickness was encapsulated in a test structure as described in [33,34]. No encapsulation was made for cell coupons with IZO, ZSO, and ALO.

DH exposure. The TMO-coated CIGS cell coupons, either bare or encapsulated in a test structure, were exposed to DH in an ESPEC environmental chamber at 85°C and 85% RH, and periodically removed for various characterization.

Characterization. The cell performances were monitored periodically by current-voltage (I-V), quantum efficiency (QE), photoluminescence (PL), and electroluminescence (EL). The samples were also photographed with a camera and examined with micro-imaging on a WYKO Optical Profiler Model 1100 interference optical microscope. XRD was performed on AZO of different thickness deposited on glass, CdS/glass, and CdS/CIGS/Mo/SLG substrates. Surface micro-morphology of DH-exposed cell coupons was analyzed with SEM.

3. RESULTS AND DISCUSSION

3.1. Optical Properties of TMOs

The T% and R% of bilayer ZnO (BZO, 0.22 μm), bilayer a-InZnO (IZO, ~0.17 μm), and single-layer a-ZnSnO (ZSO, ~0.2 μm) are shown in Fig. 1a. Depending on the thickness, the exact spectral transmittance and shape will change. For example, when the AZO increased in thickness from the standard 0.12 μm to 0.5 μm, the transmittance is reduced to certain extent; however, its effect on CIGS solar cell efficiency is not proportional to the T% loss as demonstrated previously [33]. Single layer ZSO at 0.2 μm appears similar to the BZO but with a larger absorption in the 400--700 nm range, which would reduce cell efficiency more noticeably (see below). ALO (~0.1 μm) was not included in the figure because the film was discolored non-uniformly from contamination by out-gassing of other samples in the same batch run. The effect of the TMOs, either as an inherent part of the device structure (BZO and IZO) or as an overcoat (ZSO and ALO), on the cell QE and I-V parameters are given in Fig. 1b and Table 1, respectively. As seen, bilayer IZO window composite layer produces cell efficiency lower than that with BZO control, likely due to higher sheet resistance as indicated by the higher Rs in Table 1. Both the ZSO and ALO overcoats reduced the cell efficiency as expected because of reduced light transmission.

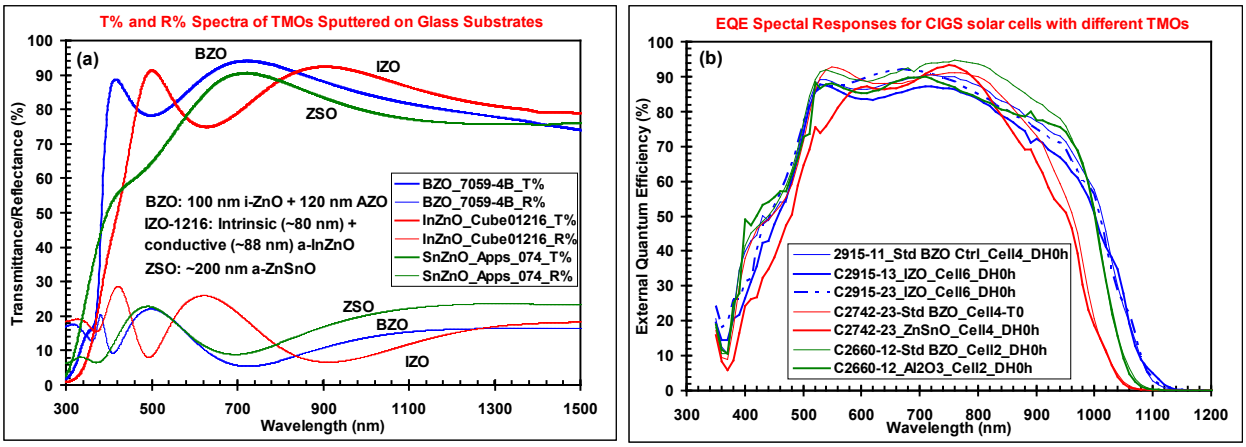

Figure 1. (a) Transmittance and reflectance spectra for bilayer ZnO (0.22 μm), InZnO (0.17 μm) and single-layer ZnSnO (0.2 μm) sputter-deposited on glass substrates. (b) External quantum efficiency spectra comparing the CIGS solar cells with IZO vs. BZO control (blue curves) as part of device structure, cell before and after ZnSnO overcoat on BZO (red curves), and cell before and after ALD Al_2O_3 overcoat (green curves).

Table 1: Examples of Cell Efficiency Change with Different TMO as Inherent Part or Overcoat

Coupon ID	Cell#	Process	TMO	Voc (V)	Jsc (mA/cm2)	FF (%)	Eff (%)	Rs (ohm-cm2)
(a) "Inherent"								
C2915-11 (Ctrl)	6	as-made	Bilayer ZnO	0.664	30.77	74.83	15.28	1.91
C2915-13	6	as-made	Bialyer InZnO	0.670	29.33	72.18	14.19	2.07
(b) a-ZnSnO Overcoat								
C2742-23	5	As-made/Au wired	Std BZO	0.725	28.88	77.47	16.22	2.06
	5		Added SnZnOx	0.730	24.19	77.66	13.72	2.56
(c) ALD Al2O3 Overcoat								
C2660-12	3	As-made/Au wired	Std BZO	0.700	30.09	67.39	14.20	2.335
	3		add ALD Al2O3	0.680	28.23	69.86	13.42	2.449
C2660-12	7	As-made/Au wired	Std BZO	0.688	31.53	75.11	16.29	2.04
	7		add ALD Al2O3	0.670	29.75	72.88	14.53	2.319

3.2 Damp Heat Stability

All the CIGS cell coupon samples with different BZO thickness, with or without encapsulation in an aluminum test structure, were exposed in one batch. The bare (unencapsulated) samples with bilayer IZO (plus a BZO control), ZSO and ALO were exposed in a second batch. The results are all negative, however — all CIGS cell coupons exhibited substantial performance degradation in DH at 85°C and 85% RH regardless of the type of metal oxides. Each TMO will be discussed individually below.

3.2.1 AZO of different thickness

Work on this study has been partly presented previously regarding the sample preparations, configurations and some of the test results [33,34]. A more detailed summary is given below, also for comparison with other TMO results. For the bare (unencapsulated) cell coupons, the samples degraded quickly with flaking of the BZO layer – the thicker the AZO the greater extent of BZO flaking and popping [33]. On the cell coupon with 0.36 µm AZO, the Au-wired contact spots were easily "bumped" off at DH = 100 h, suggesting a serious delamination issue between the Mo and SLG. In the encapsulated test structure, significant flaking of the 0.12-µm AZO layer was observed at DH = 518 h, and no significant flaking was observed for 0.50 µm AZO on one of the two cell coupons (C2529-13) until at DH = 774 h, as seen in Fig. 2. The I-V performance of the bare cell coupons exposed directly to the DH moisture degraded rapidly, as demonstrated in Fig. 3, showing efficiency and series Rs plots for some selected devices. (Data for the devices that started with low efficiency are not shown.) The two bare samples lost the efficiency essentially in a similar manner as seen in Fig. 3a. In

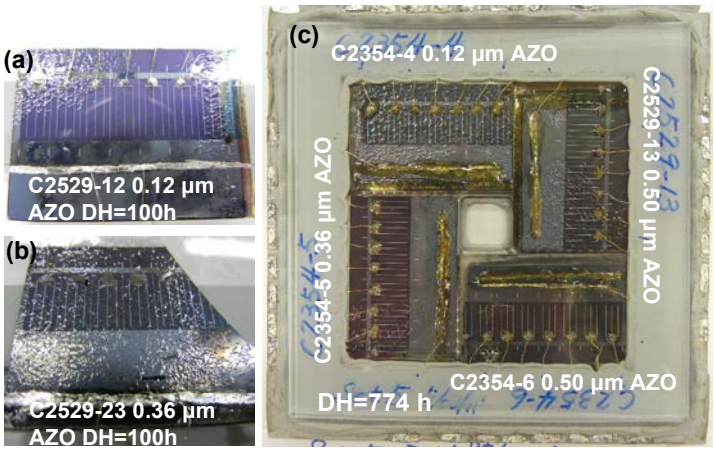

Figure 2. Photographs showing the flaking of BZO layers with different AZO thickness from 0.12 µm to 0.50 µm, as indicated, (a, b) on bare coupons and (c) in an encapsulated test structure with a TPT backsheet for moisture ingress control upon DH exposure to 100 h and 774 h, respectively. Darkening on the CIGS/Mo regions is also observed on the bare coupons. The Au wire-soldered contact on C2529-23 cell coupon was easily "bumped" off at DH = 100 h. All the CIGS cell coupons had a 0.1-µm i-ZnO layer before the Al-doped ZnO (AZO) of different thickness was sputter-deposited.

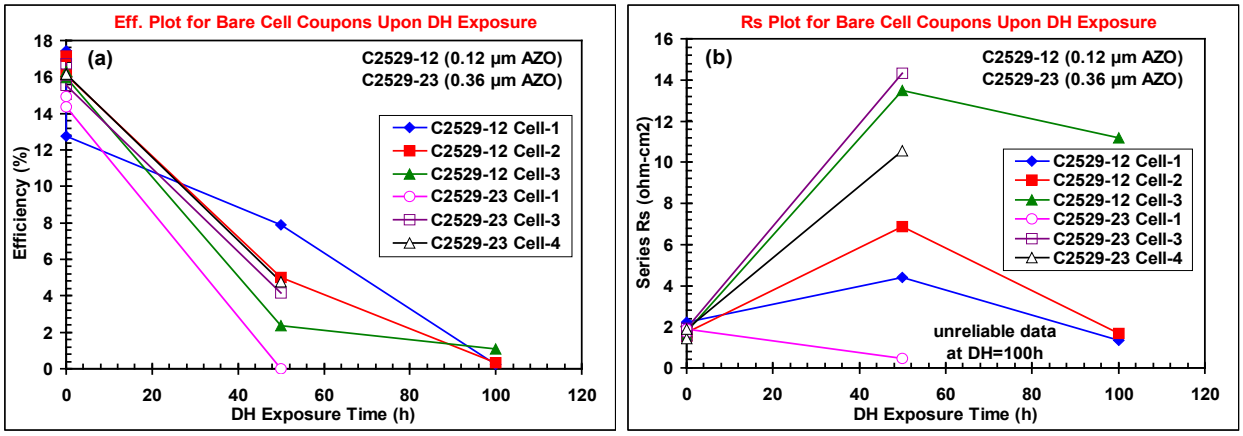

Figure 3. (a) Efficiency and (b) series Rs plots for bare cell coupons of C2529-12 with 0.12 µm AZO and C2529-23 with 0.36 µm AZO upon exposure to DH at 85°C and 85% RH. No data are available for C2529-23 at DH=100 h due to loss of Au-wire soldered contact pads. Rs data for C2529-12 at DH=100 h are unreliable due to measurement difficulty (I-V scans slowed down greatly).

the first 50 h DH exposure, the efficiency losses are coupled with similar loss pattern in Voc (not shown) and moderate to large increases in Rs (Fig. 3b). Jsc showed about 10%–30% loss for the C2529-12 (0.12 µm AZO) at DH = 100 h, and about 30%–50% for C2529-23 (0.36 µm AZO) at DH = 50 h. The faster degradation of C2529-23 appears to be affected by the substantial flaking of the BZO layer (Fig. 2b), suggesting the presence of greater mechanical stress and its detrimental effect on the thicker AZO.

Performance degradation for CIGS cell coupons with three different AZO thicknesses in the encapsulated test structure is relatively gradual because a TPT backsheet, with a WVTR of ~143 g/m^2-day measured at 86.8^{o}C and 100% RH, was employed to control the moisture ingress and hence the cell coupons are not exposed directly to the DH moisture as the bare samples. This difference is illustrated by comparing Fig. 3 with Fig. 4 below. Figure 4 presents the I-V loss for C2354-4 (0.12 µm AZO) and C2354-5 (0.36 µm), showing Voc, Jsc, efficiency, and series Rs plots, respectively, for some selected devices, upon DH exposure to 774 h. In general, except for a few devices, the Voc declined gradually as the Rs increased. The Jsc remained nearly constant until a certain turning point and then decreased quickly. The turning point was approximately at DH = 270 h for C2354-4 and at DH = 518 h for C2354-5, which corresponded to the relatively large increase in Rs. These turning points also made the efficiency's gradual loss in early stage to drop more quickly, and made the I-V measurements more difficult due to large slowdown in the scans. The I-V curve shapes could be much distorted in some cases (not shown). The results shown in Fig. 4, along with those devices not shown, also indicate the high degree of variation (or inconsistency) in the device stability even on a 1" x 1.5" cell coupon, which also makes the interpretation of the results quite challenging.

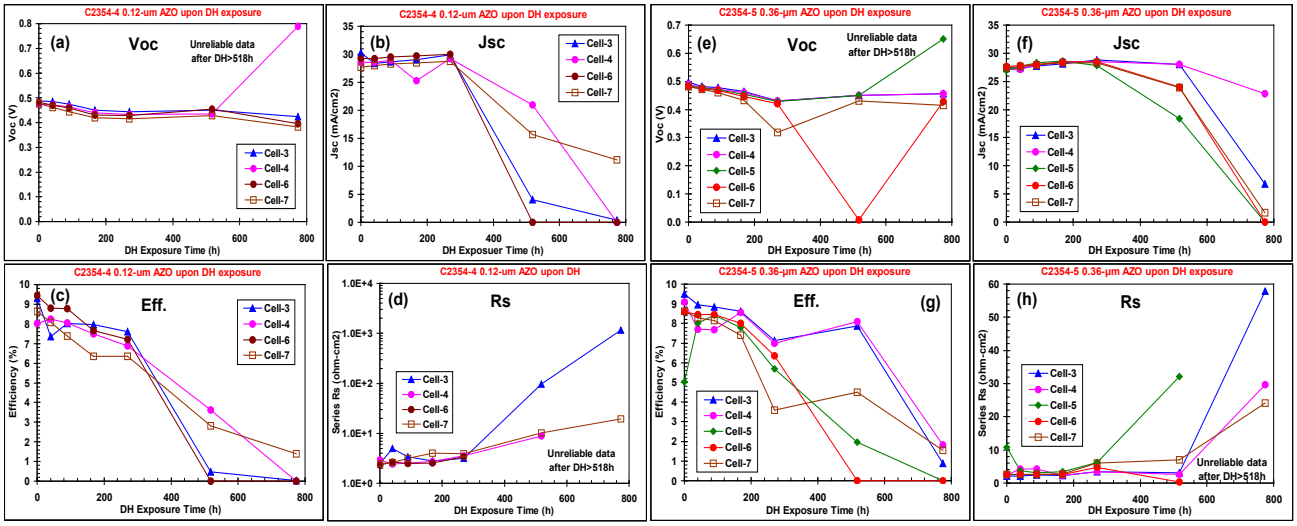

Figure 4. I-V parameter Voc, Jsc, efficiency, and series Rs plots for (a-d) C2354-4 with 0.12 µm AZO and (e-h) C2354-5 with 0.36 µm AZO in an encapsulated test structure [33,34] upon DH exposure to 774 h at 85^{o}C and 85% RH.

Figure 5 shows the efficiency and Jsc plots for the C2529-13 cell coupon with 0.50 µm AZO. Figures for the C2354-6 with the same AZO thickness are not shown because of high degree of variation in individual device degradation trend, even the cell coupon only displayed BZO flaking on a small area (Fig. 2c). Other than cell #3, which became unsteady after DH>200h and degraded rapidly, three cells showed higher loss rate in efficiency after the DH = 270 h turning point (Fig. 5a). Meanwhile, these three cells showed a quick drop in Jsc after the DH = 518 h turning point (Fig. 5b). In comparison, cell #1 exhibited a gradual decrease in both efficiency and Jsc. A notable behavior in Jsc plot is that cell #6 produced a Jsc of 35–45 mA/cm^2 before DH = 300 h, which was much higher than the average ~28 mA/cm^2. This abnormal Jsc was also seen on cells #1 and #6 of C2354-6 (0.50 µm AZO), which showed a large increase from initial ~28 mA/cm^2 at DH = 0 h to ~45 and 53 mA/cm^2 respectively at DH = 168 h. The reason for these unusual and fluctuating Jsc values is not very clear, but likely caused by a "cross-talk" of the cells with neighboring regions or cells either due to incomplete cell isolation during photolithographic processing initially or a short-term "conductive link" by the moisture and corrosion products upon DH exposure later.

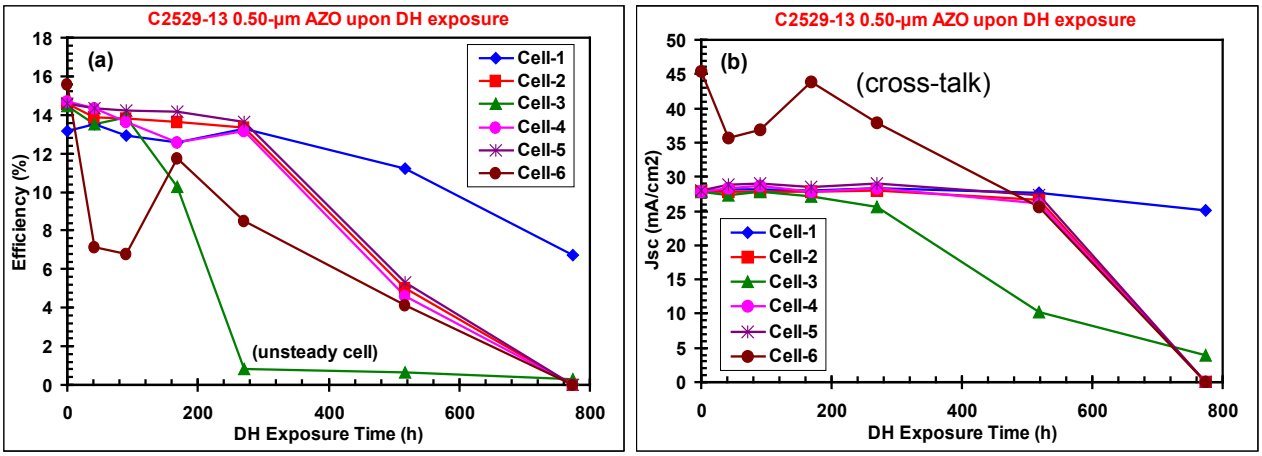

Figure 5. (a) Efficiency and (b) Jsc plots for the six devices on the C2529-13 coupon with 0.50 µm AZO in an encapsulated test structure upon exposure to DH at 85°C and 85% RH.

An important observation in this study is the contradiction of the AZO "thickness" (or substrate) effect: In previous study, when deposited on glass substrates, the AZO showed high DH stability as its thickness increased to 0.50 µm [6]. This was the underlying reason for using thicker AZO as the "inherent" moisture barrier. However, all the results from the current study discussed above show the thicker AZO layers did not offer the protection for CIGS solar cells against DH as expected. While the exact causes remain not well understood, one plausible factor is the substantially poorer crystallinity for the AZO when deposited on top of the CdS/CIGS layer. Figure 6a shows the XRD (002) peaks for the BZO layers with different thickness sputter-deposited on glass. For BZO with a 0.12 µm AZO (i.e., "group 1"), smaller (002) peak intensity was observed on the CBD CdS-coated glass. Figure 6b compares the (002) peak intensity for 16 BZO samples on various substrates, which include the cell coupon samples used in this study. The results are very obvious: the BZO (or AZO) deposited on CdS/glass and CdS/CIGS substrates tends to give weaker (002) peak intensity, indicating significantly lower crystalline quality than the AZO deposited on bare glass at the same thickness. This may further suggest the influential effects of crystalline and grain size against DH exposure.

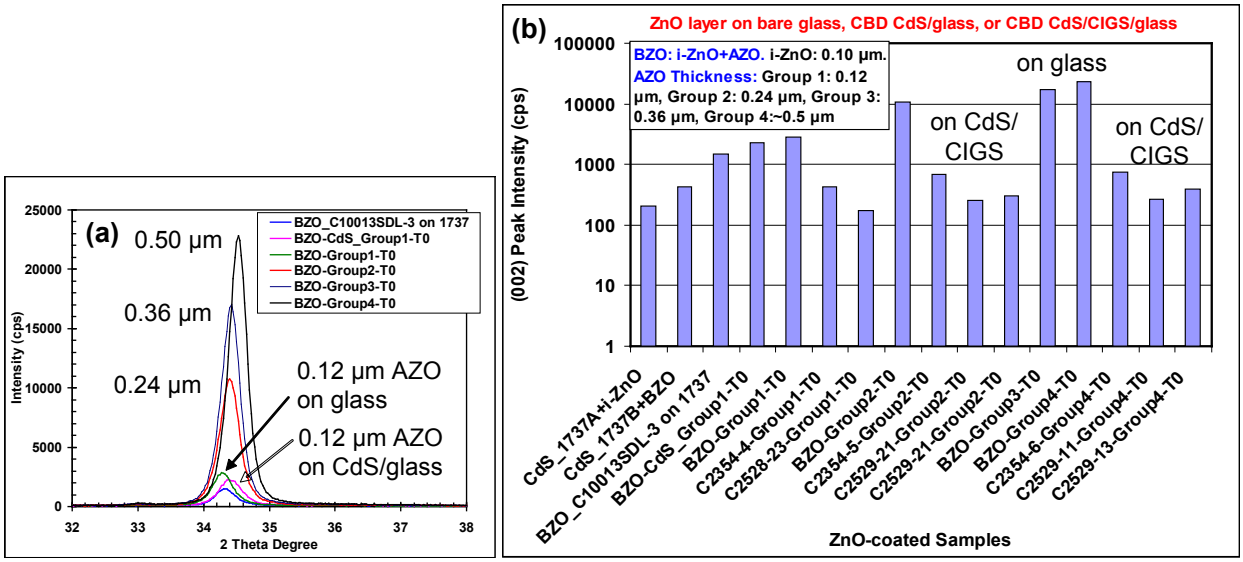

Figure 6. (a) XRD plots showing ZnO (002) peaks for six bilayer ZnO (BZO) films with 0.1 µm i-ZnO and increasing AZO thickness from 0.12 µm (group 1), 0.24 µm (group 2), 0.36 µm (group 3), and ~0.50 µm (group 4) sputter-deposited on glass and a CBD CdS-coated glass. (b) A summary plot of (002) peak intensity for 16 BZO-coated samples, ranging from glass, CdS/glass, to CdS/CIGS cell coupons, having different AZO thickness as marked by group 1 to group 4.

3.2.2 Bilayer amorphous InZnO (IZO) as the window layer

Similar to the thicker AZO on glass substrates, single-layer and/or bilayer InZnO (IZO) sputtered on glass substrates alone or over i-ZnO/glass were found in previous study to be DH stable [5,6], although the i-ZnO underlayer appeared to still be affected by the moisture permeated through the IZO overcoat [6]. We previously investigated its application as a moisture barrier film on standard BZO/CIGS device structure [35], and as the conductive window layer to replace the AZO [36]. The basics, the optical and electrical properties of the amorphous IZO (and ZSO), and the effects of preparation conditions have been extensively studied by Perkins and coworkers [37-40]. In the present study, bilayer IZO, consisting a resistive IZO and a conductive IZO, was used as the window layer, replacing the typical BZO on the CIGS solar cells. Four CIGS cell coupon samples from the same CdS/CIGS/Mo/SLG film substrate were prepared with bilayer IZO layers that were sputtered using somewhat different conditions in order to achieve good efficiency. A control with standard BZO was also prepared from the same CdS/CIGS/Mo/SLG substrate for comparison. The five samples, along with a ZSO-coated and an ALD ALO-coated sample (see below), were exposed to DH and characterized simultaneously.

As shown in Fig. 7, which compares two IZO/CIGS coupons with the BZO/CIGS control, the latter exhibited flaking of the BZO layer, similar to that seen in Fig. 2, on the left side of the coupon at DH = 48 h. The flaking spread further and to the right at DH = 110 h. In comparison, the four IZO/CIGS coupons did not show flaking behavior. Instead, they showed darkening stains commonly starting at the device isolation lines that spread wider as the exposure time increased to DH = 110 h. The darkening stains seem to be an "edge" effect and are suspected to be a result of corrosion due to ingress of moisture through the IZO layer. All the IZO/CIGS devices on the four cell coupons showed a quick large loss in efficiency in the first 24 h of DH, then recovered in later stages, as illustrated in Fig. 8. A couple of devices at DH = 110 h even showed an efficiency higher than the initial values (e.g., Fig. 8b, cell #2), apparently faulty results. These behaviors were not observed on the BZO/CIGS control, however, which showed gradual decrease in efficiency (Fig. 8a). In fact, the I-V measurements became more and more difficult to obtain good and reliable curves because the series resistance increased substantially (not shown), and the I-V parameters were not reliable in later stage when DH ≥ 72 h. For examples, some devices even showed Jsc in the 45–100 mA/cm^2 range (when measured using a constant cell area of 0.42 cm^2). The majority of the devices showed gradual to moderate losses in Voc and Jsc, but relatively obvious increase or fluctuations in Rs. Accordingly, it is suspected that the recovery in cell efficiency shown in Fig. 8(b-e) was probably a result of mutual "cross-talk" of neighboring cells or region, i.e., current contribution from the neighboring cells or regions due to certain "conductive link" at the device isolation lines or edges effected by hydrolytic corrosion of IZO, similar to that in Fig. 5b above. At DH = 110 h, the EQE for most of the IZO/CIGS devices was very low at ~1 %, a large drop from original 80%~90% in the spectral range of 500–800 nm, as seen in Fig. 8f. If the efficiency and Jsc were truly as measured for individual devices at DH = 110 h, then their EQE would show small changes, similar to that for the control.

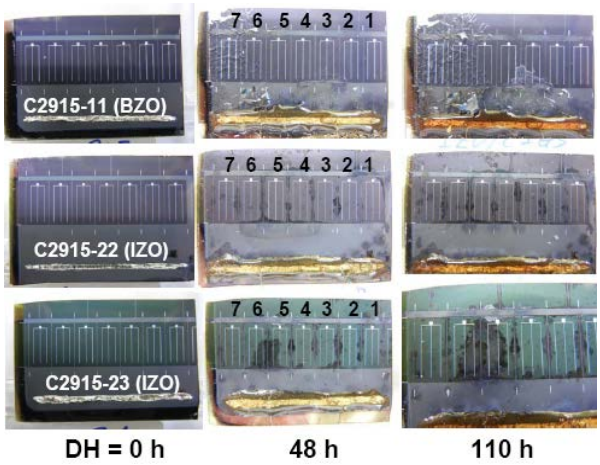

Figure 7. Photographs showing the topical appearance of three samples at DH = 0 h (left), 48 h (middle) and 110 h (right). The samples are C2925-11, the control with standard bilayer ZnO, BZO (top row); C2915-22 (middle row) and C2915-13 (bottom row) with bilayer ZnO. The base contact In strips on the sample were coated with epoxy to minimize potential damage by the damp heat at 85^{o}C and 85% RH.

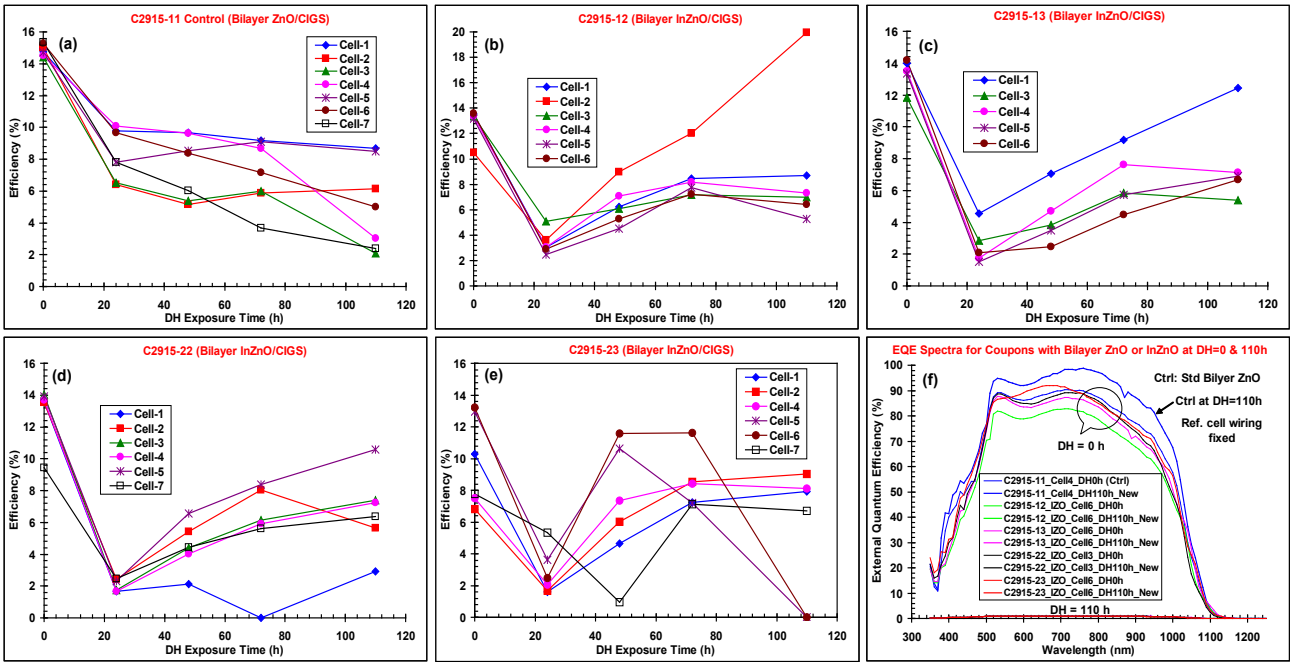

Figure 8. Efficiency plots as a function of DH exposure time for (a) C2915-11, the control with standard BZO and (b-e) the four cell coupons with bilayer IZO, C2915-12, 13, 22, and 23. (f) EQE for the control (blue curves) and some IZO/CIGS devices at DH = 0 h and 110 h. The EQE at DH = 110 h for the control appeared higher than that at DH = 0 h after the wiring of the reference cell was fixed.

PL and EL imaging was also performed for the DH-exposed IZO/CIGS samples and the BZO/CIGS control to examine if the CdS/CIGS junctions on the devices were still active and the cell areas being damaged by the DH exposure as well as if the electrical connection through the entire device was affected by the presence of high contact resistance (via EL intensity) due to degraded BZO, IZO, and AlNi grids. The results are partially illustrated in Fig. 9, showing the PL and EL images for the control and some arbitrarily chosen devices on two IZO/CIGS coupons, C2925-2 and C2915-23, at DH = 110 h. Their corresponding photographs are given in Fig. 7 (right colum) above. As revealed by the PL imaging, the CdS/CIGS junctions of the seven devices on the control were mostly PL-active after 110 h DH exposure, despite some dark spots on the cell areas and some small dark areas by the isolation lines and top edges between cell#2 and cell#5, which could not be readily revealed from the photograph (Fig. 7). On the other hand, the large EL images for the cells #1, #4, and #6 do show more clearly the damages caused by DH on the devices. For example, while both are PL-active, the lower right corner on cell#4 (upper right in the image) and the majority of cell#6 are EL-inactive, which correspond well with the large corrosion stain (cell#4) and extensive flaking (cell#6) seen in Fig. 7, clear evidence of the presence of high resistance over those dark areas caused by DH-degraded BZO (and likely AlNi grids as well) [34]. For IZO/CIGS samples, similar results are observed: most devices remained PL-active, but some areas around the edges and isolation lines by the devices are both PL- and EL-inactive (shown as dark spots or regions). These dark spots or areas correspond to the dark stains seen in the photographs of Fig. 7.

The results discussed above indicate that the bilayer IZO made for this study did not offer good DH stability to the CIGS solar cells as one would expect (or desire) from its high DH stability when present on glass substrates [6]. A likely reason is that the IZO bilayers on all four cell coupons allowed the moisture to penetrate through, resulting in hydrolytic corrosion (seen visually as the stains) that might have transformed the originally conductive films into resistive ones. For reason not clearly known at the moment, this degrading behavior appeared to be more profound starting at the isolation lines or cell edges.

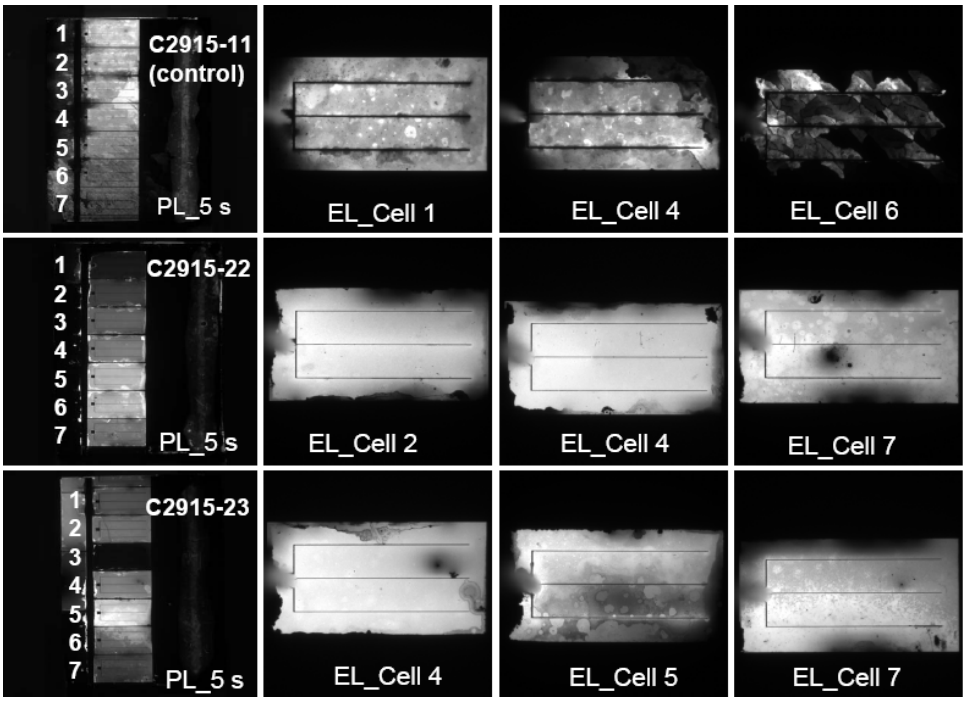

Figure 9. PL images for all devices (left column) and EL images for some arbitrarily chosen devices (as marked) on three cell coupon samples: C2915-11, the BZO/CIGS control (top row), C915-22 (middle row), and C915-23 (bottom row) of bilayer IZO/CIGS. PL images were taken with 5 s integration time, and EL images were taken at 10 mA bias with varying voltage and a 10 s integration time.

3.2.3 Single-layer amorphous ZnSnO as an overcoat

Depending on the optical and conductivity properties, amorphous ZnSnO (ZSO) can be used in different applications. For example, Hultqvist et al. used highly resistive ALD ZSO as the buffer layer for CIGS solar cells and, with a [Sn]/[Zn+Sn] ratio of 0.15-0.21, achieved a best cell efficiency of 15.3%, as compared with a 15.1% cell efficiency using the typical CdS buffer [41]. The ZSO buffer layer also demonstrated a good stability when tested in dry heat at 85^{o}C. In this work, a 0.2-µm ZSO layer was used as an overcoat on the standard BZO/CIGS solar cell in an attempt to determine its protective effectiveness for the CIGS solar cell against DH exposure at 85^{o}C and 85% RH. However, no prior study was conducted to determine if the ZSO sputtered on glass substrates would be as DH-stable as the IZO. As noted in Section 3.1 above, the 0.2-µm ZSO film on glass substrate showed a significant absorption in the 400–700 nm range, and hence reduced the EQE (see Fig. 1). The CIGS cell coupon with the 0.2-µm ZSO overcoat showed a bluish green color, and the color did not fade or change upon DH exposure. The DH exposure resulted in notable corrosion and light stains on cell areas and also at some device isolation lines, as illustrated in Fig. 10 (a and b) as marked in red and blue circles, which also showed up in the PL image (Fig. 10c) and were somewhat similar to that observed on the IZO/CIGS cell coupons (Fig. 7). Corrosion-induced spikes, spots, and holes were observed in the optical and PL images. Changes in the I-V parameters of the six devices on the C2742-23 coupon are given in Fig. 11, showing gradual decrease in Voc and Jsc, but fairly rapid decline in fill factor and efficiency due to large increase in Rs for most of the cells but cell #1. PL image in Fig. 10c indicates cells #2–#6 were PL-active but cell #1 was poor in PL intensity if not totally dead (i.e., CdS/CIGS p-n junction failed). However, EL imaging indicates only cell #1 (at a high bias of 110 mA, Fig. 10d) was EL-active, and all the others were essentially EL-inactive at 50~140 mA bias. While there was no flaking as seen on bare standard BZO/CIGS coupon samples (Figs 2 and 7), the EL-inactive results suggest the presence of high Rs, which could be caused by the DH moisture permeated through the ZSO layer and degraded the BZO layer. Furthermore, Jsc, efficiency, and EQE plots shown in Fig. 11(b, d, e) indicate cell #1 was still good with low Rs (Fig. 10e) and almost no change in EQE spectral response (Fig. 10f) at DH = 200 h. In comparison, EQE of cell #5 (Fig. 10g) shows a ~10% decrease in spectral response at DH = 200 h. Therefore, as being the only particular case observed, a good explanation/interpretation is much needed for the opposite and contradictory results in I-V, QE, PL, and EL.

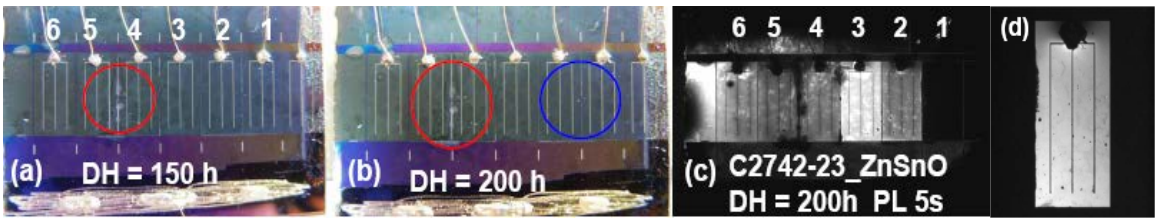

Figure 10. Photographs of the ZSO-coated BZO/CIGS cell coupon (C2742-23) at DH = 150 h (a) and 200 h (b). The DH moisture-induced corrosion and light stains are marked in the red and blue circles, respectively. (c) PL image of the coupon at DH = 200 h with 5 s integration time. (d) EL image of cell #1 at 110 mA bias, 700 mV, and 30 s integration time. (Cells #2 to #6 were EL-inactive when measured at 50~140 mA, 0.62~1.5V, and 30 s. Not shown.)

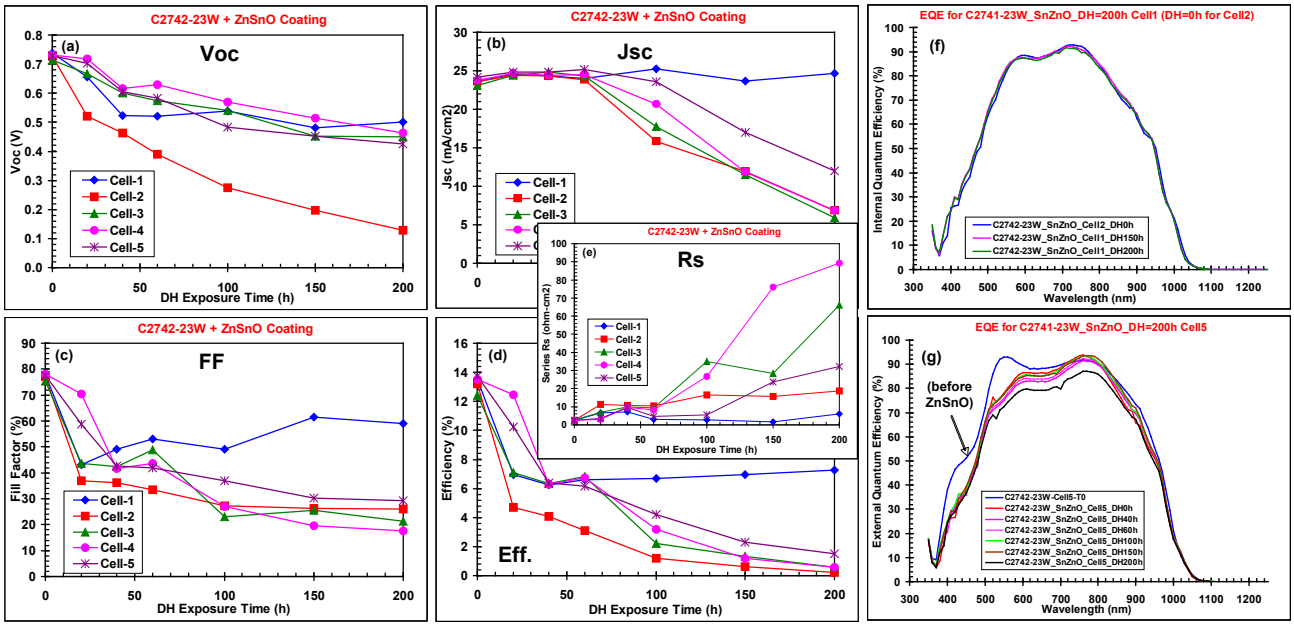

Figure 11. (a-e) I-V parameter Voc, Jsc, FF, efficiency, and series Rs plots for the ZSO-coated BZO/CIGS (C2742-23) as a function of DH exposure time. (f and g) EQE plots for cell#1 (f) and cell#5 (g) at various DH exposure times. EQE for cell#5 before (blue curve) and after (red curve) ZSO coating are shown in (g).

3.2.4 ALD Al_2O_3 as an overcoat

Thin layers of amorphous Al_2O_3 (ALO) made from atomic layer deposition (ALD) offer excellent thickness and uniformity control for their conformal and dense coating. ALD ALO has been studied as an overcoat for CIGS solar cells [42,43] as well as widely used in the fabrication of multilayer moisture barrier films [15-17, 19-21] that have been demonstrated in successfully blocking DH moisture ingress for flexible thin-film PV solar cells [15,16,20]. In this study, additional to the ZSO, we investigated the usefulness of a 0.1-µm ALD ALO layer as a direct overcoat on the standard BZO/CIGS solar cells. The ALD ALO layer was deposited on a batch of substrates at ~100°C. Unfortunately, the resultant ALO was non-uniformly discolored, likely due to out-gassing contamination from other samples (as seen on the insert photograph in Fig. 13f below). In a recent sample run with 25 nm ALD ALO only for the CIGS cell coupons, no discolored coating occurred. SEM results showed that the 0.1-µm ALO layer was very smooth on the glass substrate, and was conformal but slightly granular over the 3.0-µm AlNi gridlines deposited on the glass substrates (not shown). The ALO-coated BZO/CIGS cell coupon (C2660-12) was exposed to DH simultaneously with other coupons described above.

Upon DH exposure, the discoloration quickly disappeared in the first 20 h. Micro-cracks of the ALO layer were observed under WYKO 3D micro-imaging in early stage (possibly at DH < 20 h) followed by wrinkling and flaking from the left top area of the coupon that spread further out and down, as shown in the photographs of Fig. 12 (a and b) at DH = 150 h and 200 h. However, it was not clear if the flaking began from the BZO (as shown in Fig. 2) or from the ALO layer pulling off the BZO layer underneath along with it. The appearance of extensive micro-cracks indicated that the ALO layer might possess high mechanical stress that was relieved (likely by tensile strain) in DH [44]. The micro-cracks could induce hydrolysis of the ALO and BZO, resulting in volume expansion and hence tensile strain. PL image for the C2660-12 sample at DH = 200 h is given in Fig. 12c, showing the cell areas under the flaked area were PL-inactive (dark portion between cells #4 and #7), as being highly damaged by the DH attack. This suggests that the flaking of the ALO/BZO layers may have also pulled off the CdS, resulting in failure of CdS/CIGS junction. EL imaging only showed cell#3 to be weakly EL-active but better than other cell areas without severe DH damage (not shown), further indicating the underlying BZO layer was highly degraded. The micro-cracks, wrinkling/flaking, delamination, and corrosion of the ALD ALO layer apparently permitted moisture penetration. The relationship between ALD ALO thickness, strain/stress, and micro-cracking and its moisture-blocking properties have been extensively studied by the George group [45-47]. A thickness of < 30–40 nm was shown to be considerably less prone to micro-cracking [46,47]. Thus, the 0.1-µm ALD ALO layer used in this study was likely too thick. Samples of BZO/CIGS coupons with a thinner ALO layer at 25 nm were therefore prepared but have not yet been subjected to DH stability test. The devices on C2660-12 lost Voc, Jsc, FF, and efficiency in a gradual manner mainly due to Rs increase, as illustrated in Fig. 13, caused by ZnO and AlNi grid degradation by DH. EQE plots given in Fig. 13f show the spectral responses before and after ALD ALO coating for cell#7 and its temporal decrease upon DH exposure. An interesting observation is that the cell's QE actually became better upon coating of the discolored ALO, although other cells, e.g., cell#1, showed a decrease with mostly clear ALO overcoat due to reduced light transmission as expected.

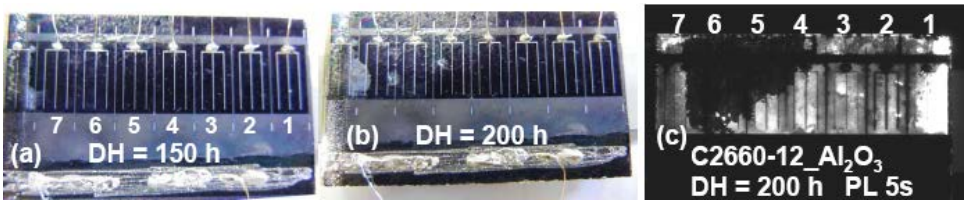

Figure 12. Photographs of the ALD Al_2O_3-overcoated standard BZO/CIGS coupon, C2660-12, at (a) DH = 150 h and (b) 200 h. (c) PL image of the C2660-12 coupon at DH = 200 h.

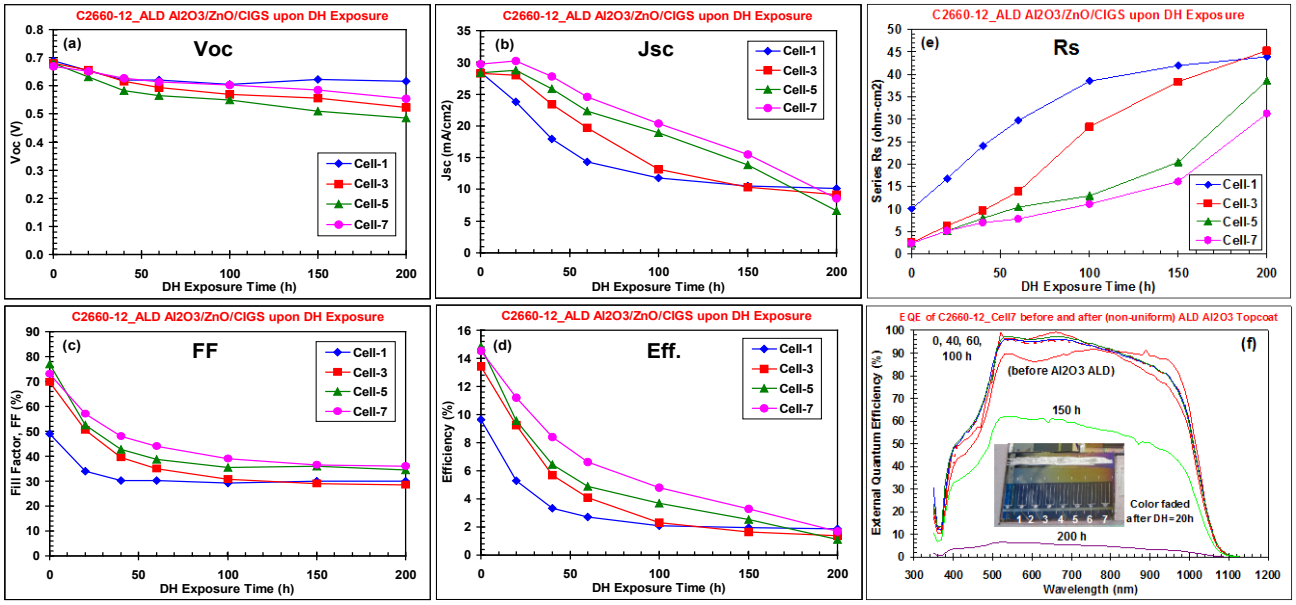

Figure 13. (a-e) I-V parameter Voc, Jsc, FF, efficiency, and series Rs plots for the ALD ALO-coated BZO/CIGS (C2660-12) as a function of DH exposure time. (f) EQE plots for cell#7 at various DH exposure times.

3.2.5 SEM micrographs for DH-exposed cell coupons

In addition to the optical photographs, I-V and PL/EL measurements, the samples were examined intermittently with a WYKO interference optical microscope to obtain 3D micrographs over the course of DH exposure. Surface morphology of the AZO, IZO, ZSO, and ALO layers all showed substantial changes due to hydrolytic corrosion, flaking, or cracking (not shown). The surface morphology of the coupons after the conclusion of DH exposure was further examined with SEM as a whole (without cutting up the cell coupons into small pieces), which offered more definite details than the WYKO images. A few of the SEM micro-images are given in Fig. 14, showing the surface morphology for each of the TMOs, with two images grouped vertically. The images can be cross-referenced with the photographs shown in Figs. 7, 10, and 12. For the standard BZO on C2915-11 control, cracking, flaking, popping and delamination are seen. For IZO on C2915-22, smearing likely due to hydrolytic corrosion and cracking are seen. Corrosion appears to be profound on ZSO surface, while large cracking and nodular growth on ALO are observed. These SEM images provide a good support of the reasoning in previous sections that corrosion, flaking/cracking, and delamination are fairly common causes that allowed the DH moisture to diffuse/penetrate and degrade the TMO windows (AZO and IZO) and/or the BZO under the overcoats (ZSO and ALO).

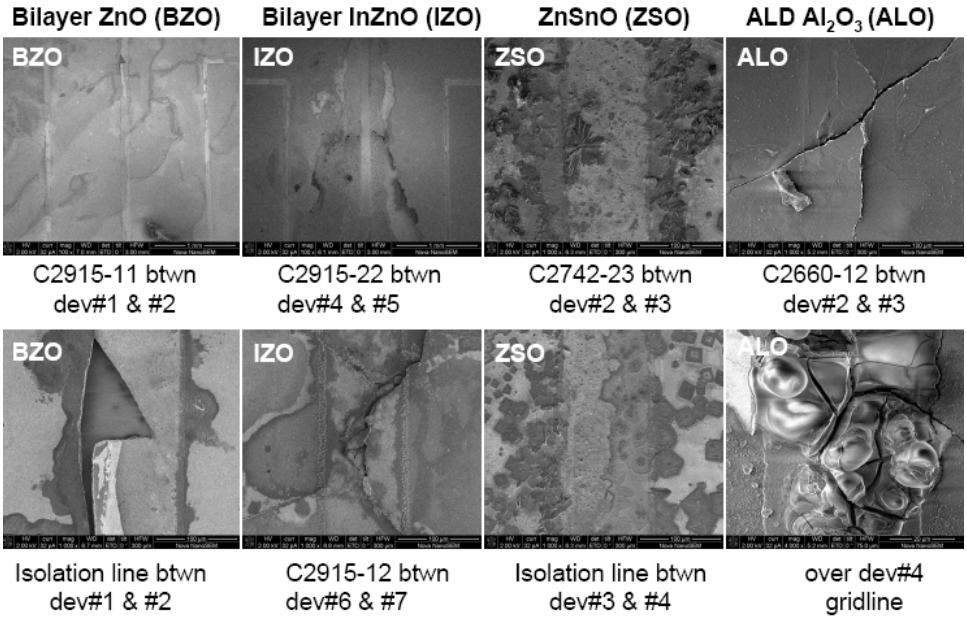

Figure 14. SEM micrographs showing the surface morphology of the TMO after DH exposure. The images were taken for the areas between two cells, at the device isolation line, or over the gridline, as indicated below each image. Two images for each TMO are grouped vertically: (a) BZO on C2915-11 control at DH = 110 h, (b) IZO on C2915-22 at DH = 110 h, (c) ZSO on C2742-23 at DH = 200 h, and ALD ALO on C2660-12 at DH = 200 h. The image size bars are 500 nm or 1 μm.

4. CONCLUSIONS

We have conducted a comparison study in an effort to identify the transparent metal oxide (TMO) materials, either as an "inherent" part of the device structure (thick Al-doped ZnO, AZO, and bilayer amorphous InZnO, IZO, to replace the standard bilayer ZnO, BZO) or as an overcoat on standard BZO/CIGS solar cells using single-layer ZnSnO, ZSO, or ALD Al_2O_3, ALO. The results from exposure to DH at 85^{o}C and 85% RH for the TMO-coated CIGS solar cell coupons are negative. All CIGS devices are degraded to certain level. Combining the optical photographs, PL and EL imaging, 3D micro-imaging (not shown), and SEM surface micro-morphology, coupled with XRD, I-V and QE measurements, the causes of the device degradations are attributed to hydrolytic corrosion, flaking, micro-cracking, and delamination induced by the DH moisture. However, these are essentially first attempts without any optimization of the TMO deposition conditions. Further studies are needed to greatly improve the DH-protective effectiveness of the TMOs. For

example, an improvement in the crystalline of thick AZO and a thinner ALD ALO to avoid micro-cracking tendencies [45-47] may be effective. Finding a good way to effectively reduce or release the internal stress for the TMOs is also highly desirable [44]. Currently, a set of new CIGS solar cell samples with 0.5 μm AZO, bilayer IZO, and 25 nm ALD ALO has been prepared to address the "edge" effect [32] that occurred at the device isolation lines and cell edges, as observed mostly on ZnO, IZO, and ZSO-coated samples, as well as the stress-cracking issue on ALO.

ACKNOWLEDGMENTS

We thank T. Gennett, A. Dameron, and M. van Hest for depositing the IZO, ALO, and ZSO films, respectively, M. Scott for photolithographic processing of the cell coupons, and S. Johnston for support on the PL and EL imaging work. This work was performed at the National Center for Photovoltaics under DOE Contract No. DE-AC36-08GO28308 with the National Renewable Energy Laboratory.

REFERENCES

[1] K. Whitfield, "Common Failure Modes for Thin-Film Modules and Considerations toward Hardening CIGS Cells to Moisture – A "Suggested" Topic," Proc. 2010 PV Module Reliability Workshop, Feb. 16-17, 2010, Golden, CO.

[2] A. Preiss, S. Krauter, M. Schoppa, and I. Luck, "PV Module Testing – How to Ensure Quality after PV Module Certification," Photovoltaic International, 13th ed., August, 2011, pp. 166-176.

[3] J. Pern and R. Noufi, "An Investigation of Stability Issues of ZnO and Mo on Glass Substrates for CIGS Solar Cells upon Accelerated Weathering and Damp Heat Exposures," DOE SETP Review Meeting, Denver, CO, April 17-19, 2007. http://www1.eere.energy.gov/solar/review_meeting/pdfs/ p_9_pern_nrel.pdf

[4] F.J. Pern, R. Noufi, X. Li, C. Dehart, and B. To, "Damp-Heat Induced Degradation of Transparent Conducting Oxides for Thin-Film Solar Cells," Proc. 33rd IEEE PVSC, San Diego, May 11-16, 2008.

[5] R. Sundaramoorthy, F.J. Pern, C. DeHart, T. Gennett, F.Y. Meng, M. Contreras, and T. Gessert, "Stability of TCO Window Layers for Thin-Film CIGS Solar Cells upon Damp Heat Exposures – Part II," Proc. SPIE Conference: Reliability of PV Cells, Modules, Components, and Systems, 8/2-6/2009, San Diego, CA.

[6] F.J. Pern, S.H. Glick, X. Li, C. DeHart, T. Gennett, M. Contreras, and T. Gessert, "Stability of TCO Window Layers for Thin-Film CIGS Solar Cells upon Damp Heat Exposures – Part III," Proc. SPIE Conference: Reliability of PV Cells, Modules, Components, and Systems, 8/2-6/2009, San Diego, CA.

[7] F.J. Pern, S.H. Glick, R. Sundaramoorthy, B. To, X. Li, C. DeHart, S. Glynn, T. Gennett, R. Noufi, and T. Gessert, "Damp-Heat Instability and Mitigation of ZnO-Based Thin Films for $CuInGaSe_2$ Solar Cells," Proc. 35 IEEE PVSC, 6/20-25/2010, Honolulu, Hawaii.

[8] F.J. Pern, B. Egaas, B. To, C.-S. Jiang, J.V. Li, S. Glynn, and C. DeHart, "A Study on the Humidity Susceptibility of Thin-Film CIGS Absorber," Proc. 34 IEEE PVSC, 6/7-12/2009, Philadelphia, PA.

[9] J. Wennerberg, J. Kessler, M. Bodegard and L. Stolt, "Damp Heat Testing of High Performance CIGS Thin Film Solar Cells," Proc. 2nd World Conference and Exhibition on Photovoltaic Energy Conversion, July 6-10, 1998, Vienna, Austria, pp. 1161-1164.

[10] J. Wennerberg, J. Kessler, and L. Stolt, "Degradation mechanism of $Cu(In,Ga)Se_2$-based thin film PV modules." Proc. 16th European Photovoltaic Science and Engineering Conference, Glasgow, 2000, pp. 309–312.

[11] J. Klaer, R. Klenk, A. Boden, A. Neisser, C. Kaufmann, R. Scheer, H.-W. Schock, "Damp Heat Stability of Chalcopyrite Mini-Modules: Evaluation of Specific Test Structures," Proc. 31st IEEE PVSC, 2005, pp. 336-339.

[12] R. Feist, S. Rozeveld, M. Mushrush, R. Kaley, B. Lemon, J. Gerbi, B. Nichols, R. Nilsson, T. Richardson, S. Sprague, R. Tesch, S. Torka, C. Wood, S. Wu, S. Yeung, and M. T. Bernius, "Examination of Lifetime-Limiting Failure Mechanisms in CIGSS-based PV Minimodules under Environmental Stress," Proc. 33rd IEEE PVSC, San Diego, CA, May 11-16, 2008.

[13] R. Feist, S. Rozeveld, B. Kern, J. D'Archangel, S. Yeung, and M. Bernius, "Further Investigation of The Lifetime-Limiting Failure Mechanisms of CIGSS-Based Minimodules Under Environmental Stress," Proc. 34th IEEE PVSC, Philadelphia, PA, June 7-12, 2009.

[14] L. Olsen, S. Kundu, M. Gross, and A. Joly, "Damp Heat Effects on CIGSS and CdTe Cells," Proc. DOE SETP Review Meeting, Denver, CO., April 17-19, 2007.

[15] L.C. Olsen, M.E. Gross, G.L. Graff, and S.N. Kundu, "Approaches to Encapsulation of Flexible CIGS Cells," Proc. SPIE Conference: Reliability of PV Cells, Modules, Components, and Systems, 8/11-13/2008, San Diego, CA.

[16] L.C. Olsen, M.E. Gross, S.N. Kundu, and W.N. Shafarman, "Properties of encapsulated Cu(In,Ga)Se_2 cells in 85°C/85%RH", Proc. 33rd IEEE PVSC, San Diego, CA, May 11-16, 2008.
[17] S. Graham, "Approaches to Barrier Coatings for the Prevention of Water Vapor Ingress," Proc. 2010 PV Module Reliability Workshop, 2/18-19/2010, Golden, CO.
[18] I. Repins, F.J. Pern, R. Sundaramoorthy, N. Bosco, T. Gennett, J. Perkins, S. Christensen, A. Dameron, L. Simpson, J. Del Cueto, S. Glick, A. Goodrich, M. Woodhouse, and T. James, "Goals and Strategies for Moisture-Hardening the CIGS device," Proc. 2011 PV Module Reliability Workshop, 2/16-17/2011, Golden, CO.
[19] Vitex Systems press release, "Vitex Systems Achieves Lifetime Record on Flexible Copper Indium Gallium Selenide Solar Cells," http://www.vitexsys.com/new/index.php?action=release-detail&PRID=33, June 12, 2008.
[20] Tracie Berniard, "Demonstrating Reliability of Ultra Barrier Solar Films for Flexible PV Applications," Proc. 2012 PV Module Reliability Workshop, 2/28-3/1/2012, Golden, CO.
[21] K. W. Leffew, S. Boussaad, D. Reardon, H. Tate, N. Glassmaker, D. Dean, G. Nunes, C. Q. Zhao, S.L. Samuels, J. SChnieder, P. Garcia, R. McLean, "Systems Approaches to High Performance CIGS Material Set including Flex Ultra-Moisture Barrier and Hi-Temp MILI Substrate," Proc. 2011 PV Module Reliability Workshop, Golden, CO.
[22] M. Kempe, D. Panchagade, A. Dameron, and M. Reese, "Predicting the Performance of Edge Seal Materials for PV," 2012 PV Module Reliability Workshop, 2/27-3/1/2012, Golden, CO.
[23] D. J. Coyle, H. A. Blaydes, J. E. Pickett, R. S. Northey, and J. O. Gardner, "Degradation Kinetics of CIGS Solar Cells," Proc. of 35th IEEE PVSC, 2009, pp. 1943-1947.
[24] D. J. Coyle, H. A. Blaydes, J. E. Pickett, T. Tolliver, R. S. Northey, R-A Zhao, and J. O. Gardner, "Packaging Requirements for ITO-Hardened CIGS," 2010 PV Module Reliability Workshop, 2/18-19/2010, Golden, CO.
[25] D. J. Coyle, "Life Prediction for CIGS Solar Modules, Part 1: Modeling Moisture Ingress and Degradation," Prog. Potovolt: Res. Appli., 2011, published online in Wiley Online Library (wileyonlinelibrary.com). DOI: 10.1002/pip.1172.
[26] D. J. Coyle, H. A. Blaydes, R. S. Northey, J. E. Pickett, K. R. Nagarkar, R-A Zhao, and J. O. Gardner, "Life Prediction for CIGS Solar Modules, Part 2: Degradation Kinetics, Accelerated Testing, and Encapsulant Effect," Prog. Photovolt: Res. Appl., 2011, published online in Wiley Online Library. DOI: 10.1002/pip.1171
[27] S.H. Glick, J.A. del Cueto, K. Terwilliger, G. Jorgensen, B.M. Keyes, L.M. Gedvilas, and F.J. Pern, "Silicon Oxynitride Thin Film Barriers for PV Packaging," Poster presentation, Proc. DOE SETP Review Meeting, Denver, CO, Nov. 7-10, 2005.
[28] J.A. del Cueto, S.H. Glick, G. Jorgensen, K. Terwilliger, and M. Kempe, "Efficacy of Thin Film Silicon Oxynitride as Water-Resistant Barriers on Photovoltaics Cells, PET, and Aluminum-coated Mirrors," NREL Test Report #TR05PVSiOxNy.001, Dec. 12, 2005.
[29] X. Li, F.J. Pern, S. Glick, and R. Noufi, "Protective Metal Oxides for CIGS Thin-Film Solar Cells," NREL Record of Invention (ROI) #09-70, August 2009.
[30] M. W. DeGroot, P. R. Elowe, and M. Stempki, "Barrier Technology Providing Exceptional Stability for CIGS Devices under Accelerated Damp Heat Conditions," Proc. 35th IEEE PVSC, 6/20-25/2010.
[31] B. S. Tosun, R. K. Feist, A. Gunawan, K. A. Mkhoyan, S.A. Campbell, and E. S. Aydil, "Improving the Damp Heat Stability of Copper Indium Gallium Diselenide Solar Cells with a Semicrystalline Tin Oxide Overlayer", Solar Energy Materials & Solar Cells, 101 (2012) 270-276.
[32] C. P. Thompson, S. Hegedus, P. F. Carcia, and R. S. McLean, "The Effects of Device Geometry and TCO/Buffer layers on Damp Heat Accelerated Lifetime Testing of Cu(In,Ga)Se_2 Solar cells," Proc. 2012 PV Module Reliability Workshop, Golden, CO., and Proc. 38th IEEE PVSC, 6/3-8/012, Austin, TX.
[33] F.J. Pern, L. Mansfield, C. DeHart, S.H. Glick, F. Yan, and R. Noufi, "Thickness Effect of Al-Doped ZnO Window Layer on Damp-Heat Stability of $CuInGaSe_2$ Solar Cells," 37th IEEE PVSC, 6/21-6/25/2011, Seattle, WA.
[34] F.J. John Pern and R. Noufi, "Characterization of Damp-Heat Degradation of $CuInGaSe_2$ Solar Cell Components and Devices by (Electrochemical) Impedance Spectroscopy," Proc. 2011 SPIE PV Reliability Conference, 8/21-25/2011, San Diego, CA.
[35] R. Sundaramoorthy, I. Repins, D. Albin, J. Pern, X. Li, T. Gessert, T. Gennett, "Investigation of Stability Issues of TCO Barrier Layers for CIGS Devices during Damp Heat and Dry Heat Exposures," Bulletin of APS, Vol. 54, paper # X12.00002, 3/16-20/2009, Pittsburgh, PA.
[36] R. Sundaramoorthy, I. L. Repins, T. Gennett, F. J. Pern, D. Albin, Jian V. Li, C. DeHart, S. Glynn, J. D. Perkins, D.S. Ginley, and T. Gessert, "Comparison of Amorphous InZnO and Polycrystalline ZnO:Al Conductive Layers for CIGS Solar Cells," Proc. 34th IEEE PVSC, Philadelphia, PA, June 7-12, 2009, pp. 1576-1581.

[37] J. D. Perkins and D. S. Ginley, "Transparent Conducting Oxides for Advanced Photovoltaic Applications," Photovoltaic International, 3rd ed., Feb. 2009, pp. 95-104.
[38] J. D. Perkins, T. Gennett, M. F. A. M. van Hest, L. M. Gedvilas and D. S. Ginley, "Optical Absorption and Electrical Conductivity in Amorphous In-Zn-O: A New TCO for CIGS PV," Proc. 34th IEEE PVSC, Philadelphia, PA, June 7-12, 2009, pp. 1141-1143.
[39] J. D. Perkins, T. Gennett, J.E. Leisch, R. Sundaramoorthy, I. L. Repins, M. F. A. M. van Hest, D.S. Ginley, "Amorphous Transparent Conductors for PV Applications," Proc. 35th IEEE PVSC, 2010, pp. 989-991.
[40] J. D. Perkins, T. Gennett, M. Galante, D. Gillaspie, and D. S. Ginley, "Amorphous Indium-Zinc-Oxide Transparent Conductors for Thin Film PV," Proc. 37th IEEE PVSC, 2011, pp. 3646-3648.
[41] A. Hultqvist, C. Platzer-Björkman, U. Zimmermann, M. Edoff, and T. Törndahl, "Growth Kinetics, Properties, Performance, and Stability of Atomic Layer Deposition Zn–Sn–O Buffer Layers for Cu(In,Ga)Se_2 Solar Cells," Prog. Photovolt: Res. Appl. (2011), Published online in Wiley Online Library. DOI: 10.1002/pip.1153
[42] L. J. Simpson, A. Dameron, S. Christensen, T. Gennett, M. Reese, J. Berry, J. Perkins, and D. Ginley, "Novel Transparent Conducting Barriers for Photovoltaics," Proc. 35th IEEE PVSC, 2010, pp. 1052-1056.
[43] P.F. Carcia, R.S. McLean, and S. Hegedus, "Encapsulation Of Cu(In,Ga)Se_2 Solar Cells with Al_2O_3 Thin-Film Moisture Barrier Grown by Atomic Layer Deposition", Solar Energy Materials & Solar Cells 94 (2010) pp. 2375-2378.
[44] T. Sasabayashi, P.K. Song, Y. Shigesato, K. Utsumi, A. Kaijo, and A. Mitsui, "Internal Stress of ITO, IZO, and GZO Films Deposited by RF and DC Magnetronic Sputtering," Mat. Res. Soc. Symp. Proc., Vol. 666, 2001, pp. F2.4.2-F.2.4.6.
[45] P.F. Carcia, R.S. McLean, M.D. Groner, A.A. Dameron, and S. M. George, "Gas Diffusion Ultrabarriers on Polymer Substrates using Al_2O_3 Atomic Layer Deposition and SiN Plasma-Enhanced Chemical Vapor Deposition," J. Applied Phys., 106 (2009) pp. 023533-1~6.
[46] S.-H. Jen, J.A. Bertrand, and S.M. George, "Critical Tensile and Compressive Strains for Cracking of Al_2O_3 Films Gown by Atomic Layer Deposition," J. Applied Phys., 109 (2011) 084305-1~11.
[47] S.-H. Jen, P.R. Fitzpatrick, J.A. Bertrand, Z.M. Gibbs, and S.M. George, "Flexibility of Al_2O_3 ALD Films and Scaleup using Spatial ALD," presented at seminar meeting of Rocky Mountain section of MRS, 9/28/2011, Boulder, CO.